Relaxation Dynamics of 2,7- and 3,6-Distyrylcarbazoles in Solutions and in Solid Films: Mechanism for Efficient Nonradiative Deactivation in the 3,6-Linked Carbazole

Tsai-Te Wang, Szu-Min Chung, Fang-Iy Wu, Ching-Fong Shu, and Eric Wei-Guang Diau*

Department of Applied Chemistry, Institute of Molecular Science, Center for Interdisciplinary Molecular Science, National Chiao Tung University, Hsinchu 30010, Taiwan

Received: July 18, 2005; In Final Form: October 25, 2005

We performed time-resolved spectral investigations of two distyrylcarbazole derivatives, 2,7- and 3,6-distyrylcarbazole (2,7-DPVTCz and 3,6-DPVTCz, respectively), in dilute toluene solution and in solid films mixed with poly(methyl methacrylate) (PMMA). The lifetime of 2,7-DPVTCz in its excited state in solution is ∼100 times as great as that of 3,6-DPVTCz, consistent with their photophysical nature. The former shows intense emission, but the latter is nearly nonfluorescent in a free environment. Moreover, the lifetime of 3,6-DPVTCz in its excited state increased also ∼100 times when the molecule was encapsulated in a 3,6-DPVTCz/PMMA solid film, indicating that intramolecular motion of the molecule significantly affects the observed relaxation dynamics in a confined environment. Calculations on the excited states indicate that an efficient intersystem crossing is activated upon twisting of the bridged C—C single bond in a free 3,6-linked carbazole; such efficient deactivation is impractical in 2,7-linked carbazole or for 3,6-linked carbazole in a PMMA matrix. Information obtained from experiments on femtosecond fluorescence enables us to distinguish crucial relaxation processes in the excited state for a profound understanding of the details of vibrational and electronic relaxations of 3,6-DPVTCz in solution.

1. Introduction

Small molecules and polymers containing carbazole moieties have been demonstrated to be materials that transport holes effectively because the nitrogen atom in the carbazole ring bestows an electron-donating ability.[1−6] Recently, we synthesized distyrylcarbazole derivatives and studied their physical properties for use as both hole-transporting and emitting layers in blue light-emitting diodes.[7] We designed two distyrylcarbazole derivatives with their 2,2-diphenylvinyl end groups substituted through either the 2,7- or the 3,6-position, denoted 2,7-DPVTCz and 3,6-DPVTCz, respectively; their chemical structures are shown in Chart 1. These distyrylcarbazole derivatives show bifunctional, blue-emitting, hole-transporting features for use in simple double-layer devices. We have demonstrated that the devices prepared using 2,7-DPVTCz as the emitter produced bright blue emissions having activating voltages less than 3.0 V, making them promising materials in organic light-emiting diode (OLED) applications.[8]

Carbazole derivatives have also been identified as promising antitumor agents due to their strong interaction with DNA.[9] The fluorescence of the carbazole chromophore bestows a specificity in investigation of the properties of medicinal compounds in biological systems.[10] For example, a 3,6-vinylcarbazole (BMVC) was found to be an excellent telomerase inhibitor to stabilize the G-quadruplex of human telomeres, with high sensitivity as a specific fluorescence marker of cancer cells.[11] The unique spectral feature for BMVC as a sensitive biosensor is that the fluorescence of BMVC is enhanced 10−100 times upon interaction with DNA.[11b] Although BMVC itself is scarcely fluorescent upon excitation in aqueous solution, strong emission is observable when the BMVC/DNA complex is formed.

CHART 1: Chemical Structures of 2,7- and 3,6-Linked Carbazoles

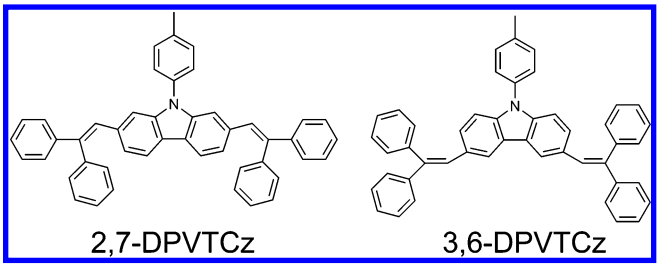

Analogously, 3,6-DPVTCz is almost nonfluorescent in dilute solution, whereas 2,7-DPVTCz shows intense emission in solution. The fluorescence quantum yield (Φ_f) of the 2,7-linked carbazole ($\Phi_f \approx 0.5$) is ∼50 times as large as that of the 3,6-linked carbazole ($\Phi_f \approx 0.01$).[7] Calculations for model carbazole systems in their excited states[7] indicate that twisting of the adjacent C—C bonds in the 3,6-position of the carbazole core causes an efficient nonradiative relaxation to occur in dilute solution. In contrast, such intramolecular deactivation from an excited state is inefficient in 2,7-linked carbazoles.

To improve our understanding of the relaxation mechanism of the carbazole system and to answer the fundamental question about the efficient nonradiative deactivation that occurs in carbazole derivatives only with π-conjugated substituents in the 3,6-position rather than in the 2,7-position, we conducted time-resolved spectral investigations for both 2,7-DPVTCz and 3,6-DPVTCz compounds in toluene solutions and in poly(methyl methacrylate) (PMMA) films. We found that the average lifetime of 2,7-DPVTCz in its excited state is $\tau_s \approx 1.4$ ns, whereas that of 3,6-DPVTCz is $\tau_s \approx 10$ ps in dilute solutions. The value of τ_s increased ∼100 times when the 3,6-DPVTCz molecule was encapsulated in a 3,6-DPVTCz/PMMA solid film,

* Author to whom correspondence should be addressed. Fax: (886)-03-572-3764. E-mail: diau@mail.ac.nctu.edu.tw

10.1021/jp053940k CCC: $30.25
Published on Web 11/24/2005

indicating that intramolecular motion of the molecule significantly affects the observed relaxation dynamics in the PMMA matrix. Calculations on the excited states indicate that an efficient intersystem crossing (ISC) is involved via curve crossing between the first singlet excited state (S_1) and the fourth triplet excited state (T_4) upon twisting of the bridged C—C single bond in a free 3,6-linked carbazole; such efficient curve crossing is impractical in 2,7-linked carbazole or for 3,6-linked carbazole in a restricted environment. Femtosecond relaxation dynamics of 3,6-DPVTCz in solution provide crucial dynamical information about the details of vibrational and electronic relaxation in this system on the S_1 potential-energy surface (PES). We proffer a mechanism for nonradiative relaxation of 3,6-DPVTCz in dilute solution according to both real-time observations and theoretical calculations.

2. Experimental Section

2.1. Materials. 2,7-DPVTCz and 3,6-DPVTCz were synthesized through Suzuki coupling from their precursors;[12−14] the detailed procedure for synthesis, purification, and characterizations is given elsewhere.[7] Samples were prepared in both solution and thin films. For solutions, 2,7-DPVTCz (or 3,6-DPVTCz) was dissolved in toluene (Merck, spectral grade) to form a homogeneous solution of concentration 1.0×10^{-5} M. To make thin films, we mixed 2,7-DPVTCz (or 3,6-DPVTCz) with a transparent polymer, PMMA, in a ratio of 1:1000 by mass. The carbazole/PMMA mixture is dissolved in chloroform (Merck, pro analysi) to form a viscous solution and then smoothly deposited onto a quartz plate via a standard spin-coating procedure.

2.2. Steady-State Spectral Measurements. UV/visible absorption spectra of samples in solution and thin films were measured with a standard spectrophotometer (Cary 50, Varian). Fluorescence emission spectra were obtained with a composite charge coupled device (CCD) spectrometer (USB2000FLG, Ocean Optics) with an excitation source shared with the same pulsed diode laser head as used in time-resolved measurements that produces excitation pulses at $\lambda_{ex} = 375$ nm with an average power of $\sim$300 μW.

2.3. Picoseond Time-Correlated Single-Photon-Counting Measurements. Picosecond time-resolved experiments were performed with a time-correlated single-photon-counting (TCSPC) system (Fluotime 200, PicoQuant) as reported previously.[15] The excitation source contains a picosecond diode laser head (LDH-P-C-375, PicoQuant) coupled with a laser diode driver (PDL-800B, PicoQuant) that produces light pulses of $\sim$70 ps at full width at half-maximum (fwhm) at a repetition rate 40 MHz. The excitation laser pulse was focused onto a solid thin film or a cuvette (thickness 1 cm) containing the sample solution. Fluorescence emitted at a right angle was collected with a lens pair. The wavelength of fluorescence was selected via a subtractive double monochromator. A microchannel-plate photomultiplier (R3809U-50, Hamamatsu) served as a photon-counting detector from which the signal was fed into a computer with a TCSPC module (SPC-630, Becker and Hickl) for data acquisition. A polarizer served to select the polarization of the emission with respect to the excitation laser pulse; in all experiments reported here the polarization was fixed at the magic-angle condition (54.7°).

2.4. Femtosecond Fluorescence Up-Conversion Measurements. The dynamics of femtosecond relaxation of the system were measured with a fluorescence optically gated (up-conversion) system (FOG100, CDP) in combination with a mode-locked Ti:sapphire laser (Mira 900D, Coherent) pumped with a 10-W Nd:YVO_4 laser (Verdi-V10, Coherent). Details of this experimental setup are given elsewhere.[16] Briefly, the femtosecond laser system generates output pulses at 740 nm with durations of $\sim$150 fs at a repetition rate 76 MHz. The frequency of the laser pulse at 740 nm was doubled for excitation ($\lambda_{ex} =$ 370). The residual fundamental pulse was used as an optical gate; a dichroic beam splitter served to separate excitation and gate beams. The excitation beam intensity was appropriately attenuated and then focused onto a 1-mm rotating cell containing the sample solution. The fluorescence was collected with two parabolic mirrors and focused on a β-barium borate (BBO) type-I crystal. The gate pulse was also focused on the BBO crystal for sum-frequency generation. The latter signal was collected with a lens and separated from interference light with an iris, a band-pass filter, and a double monochromator (DH10, Jobin Yvon) in combination, then detected with a photomultiplier (R1527P, Hamamatsu) connected to a computer-controlled photon-counting system. On varying the temporal delay between gate and excitation pulses via a stepping-motor translational stage, we obtained a temporal profile (transient). The polarization between the pump and probe pulses was fixed at the magic-angle condition (54.7°).

2.5. Data Analysis and Kinetic Model. The fluorescence transient signal, $I(t)$, was fitted through convolution of the instrument response function $g(t)$ with an appropriate molecular response function $f(t)$[17,18]

$$I(t) = \int_0^\infty g(t - s)f(s)\,ds \tag{1}$$

in which $g(t)$ is a Gaussian function; the choice of $f(t)$ relies on a proper kinetic model. When a rising feature appears in the transients, a consecutive kinetic model is employed to fit appropriately the transients

$$A \xrightarrow{\tau_0} B \xrightarrow{\tau_1} C \tag{2}$$

in which component A is described with a single-exponential function with a decay coefficient τ_0 and component B is described with a biexponential function with a rise coefficient τ_0 and a decay coefficient τ_1. The molecular response function $f(t)$ is expressed accordingly as

$$f(t) = a \exp\left(-\frac{t}{\tau_0}\right) + b\left[\exp\left(-\frac{t}{\tau_1}\right) - \exp\left(-\frac{t}{\tau_0}\right)\right] \tag{3}$$

in which the preexponential factors a and b represent the relative weights (or amplitudes) of components A and B, respectively. Alternatively, a parallel kinetic model is employed to account for the observed temporal profiles showing a biphasic dynamical feature

$$B \xrightarrow{\tau_1} C \tag{4}$$

$$B' \xrightarrow{\tau_2} C' \tag{5}$$

in which components B and B' are described with a single-exponential function and decay coefficients τ_1 and τ_2, respectively.

2.6. Computational Methods. The quantum-chemical calculations for both 2,7-linked and 3,6-linked carbazoles were performed with the Gaussian03 software package.[19] In general, geometries of molecules in the ground state were optimized at the B3LYP/6-31G(d) level of theory whereas those in the S_1 state were optimized at the CIS/6-31G(d) level of theory. Single-

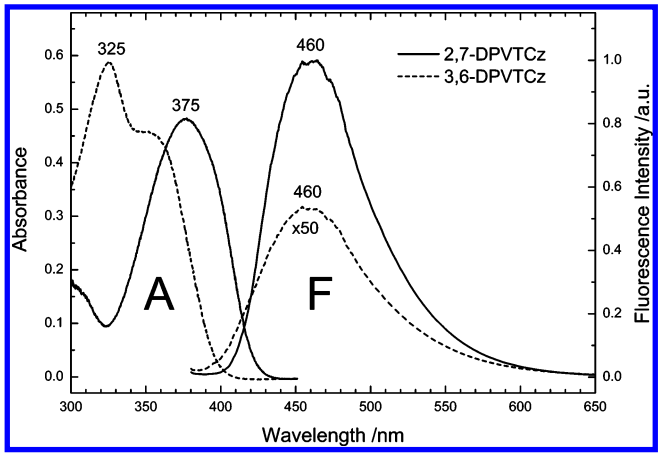

Figure 1. UV/visible absorption (A) and fluorescence (F) spectra of 2,7-DPVTCz (solid curves) and 3,6-DPVTCz (dashed curves) in dilute toluene solutions ($C = 1.0 \times 10^{-5}$ M). The relative fluorescence intensity of 3,6-DPVTCz has been scaled by a factor 50 for comparison with that of 2,7-DPVTCz.

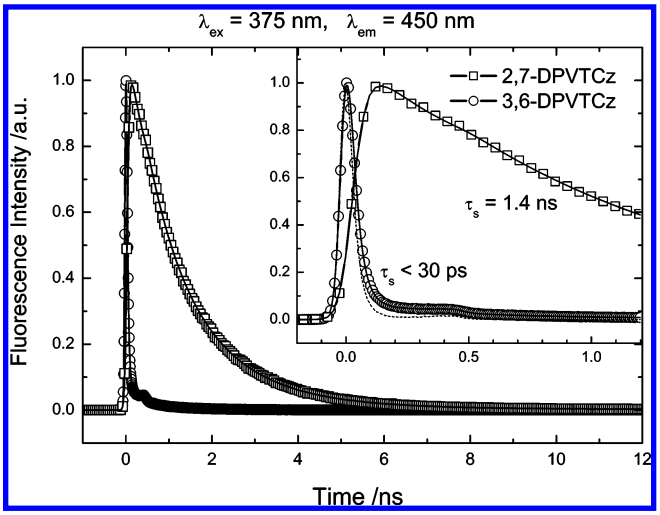

Figure 2. Picosecond fluorescent transients of 2,7-DPVTCz (squares) and 3,6-DPVTCz (circles) in dilute toluene solutions ($C = 1.0 \times 10^{-5}$ M) obtained on excitation at $\lambda_{ex} = 375$ nm and probing at $\lambda_{em} = 450$ nm. The inset shows the corresponding transients on a sub-nanosecond scale with the instrument response function shown as a dashed curve.

point calculations for excitation energies were performed with time-dependent density-functional theory (TDDFT) at the B3LYP/6-31+G(d) level.

3. Results and Discussion

3.1. Steady-State Photophysical Properties. We measured UV/visible absorption (A) and fluorescence (F) spectra of the two distyrylcarbazole derivatives in dilute toluene solutions; Figure 1 shows the corresponding spectra for 2,7-DPVTCz (solid curves) and 3,6-DPVTCz (dashed curves). The absorption maximum of 3,6-DPVTCz is located at 325 nm; i.e., it is blue-shifted by ca. 50 nm with respect to that of 2,7-DPVTCz. This shift presumably originates from the disparate lengths of conjugation that result from the varied substitution patterns of 2,2-diphenylvinyl groups on the carbazole cores. In 2,7-DPVTCz, conjugation can extend over the entire molecule, whereas in the 3,6-DPVTCz there is little conjugation over large distances. This spectral feature is similar to that of carbazole-based trimers[3] or polymers[2] in which the effective electronic conjugation length is larger in the 2,7-linked species than that in the 3,6-linked species.[20]

2,7-DPVTCz displays intense photoluminescence in the blue region, with its maximum at ~460 nm. Using quinine sulfate dihydrate/H_2SO_4 (0.5 M) aqueous solution as a standard for fluorescence quantum yield ($\Phi_f = 0.546$),[17] we determined the value of Φ_f of 2,7-DPVTCz in dilute toluene solution to be 0.57, similar to the value of 0.51 previously determined with reference to 9,10-diphenylanthracene in cyclohexane.[7] In contrast, 3,6-DPVTCz in toluene solution exhibits weak emission, with its maximum occurring also at ~460 nm (Figure 1); its fluorescence quantum yield was determined to be only ~0.01.[7] The factor 50 for Φ_f between 3,6-linked and 2,7-linked carbazoles is remarkable, and this unusual photophysical behavior between the two types was also reported in a carbazole-based trimer system.[3b] We therefore undertook time-resolved investigations to understand the relaxation mechanism of the system.

3.2. Picosecond Relaxation Dynamics in Solutions. Figure 2 displays the fluorescence transients of 2,7-DPVTCz and 3,6-DPVTCz in toluene solution obtained using the TCSPC method at $\lambda_{ex} = 375$ nm and $\lambda_{em} = 450$ nm; the other transients ($\lambda_{em} = 400-600$ nm) taken under the same conditions are provided in the Supporting Information (Figures S1−S4). The temporal profile of the 2,7-linked species has an averaged decay coefficient $\tau_s = 1.4$ ns whereas the decay coefficient of the 3,6-linked species is poorly determined because of the limit of instrumental resolution ($\tau_s < 30$ ps). This discrepancy in Φ_f between 2,7-DPVTCz and 3,6-DPVTCz is hence consistent with the observed excited-state dynamics for an efficient nonradiative relaxation channel activated in the latter case. Φ_f is related to the excited-state lifetime (τ_s) through this equation

$$\Phi_f = \tau_S k_r \tag{6}$$

in which k_r is the radiative time coefficient of the molecule. Using data extracted from Figure 1 and inserted into the Strickler−Berg relation,[21] we determined k_r to be 4.8×10^8 and 7.0×10^8 s^{-1} for 2,7-DPVTCz and 3,6-DPVTCz, respectively. The values of Φ_f are accordingly estimated to be 0.67 and <0.02 for the former and the latter, respectively; the values are consistent with those obtained from the aforementioned steady-state measurements. Picosecond time-resolved measurements have thereby confirmed the results obtained from steady-state spectral measurements and indicate the existence of an efficient channel for nonradiative relaxation that is activated in the 3,6-linked carbazole but inhibited in the 2,7-linked carbazole. To discover the nature of this nonradiative relaxation process, we performed time-resolved measurements also for the carbazole molecule without the distyryl substituents. This control experiment indicates that the carbazole core itself shows intense emission in dilute solution ($\tau_s = 6.8$ ns), implying that an efficient nonradiative relaxation would occur for the system only with π-conjugated substituents in the 3,6-position. To disclose how nuclear motion is involved in the excited-state deactivation, time-resolved measurements were conducted in carbazole/PMMA thin films in which nuclear motion of the molecule is substantially restricted within the rigid PMMA environment.

3.3. Picosecond Relaxation Dynamics in PMMA Thin Films. Figures 3A and B show absorption and fluorescence spectra of 2,7-DPVTCz and 3,6-DPVTCz in PMMA thin films, respectively; their corresponding steady-state spectra in solution are shown as dashed curves for comparison. The absorption spectra in PMMA films are similar to those in solution for both molecules, but the fluorescence spectra in PMMA films exhibit blue shifts with respect to those in solution by ~10 nm and ~20 nm for 2,7-DPVTCz and 3,6-DPVTCz, respectively. This

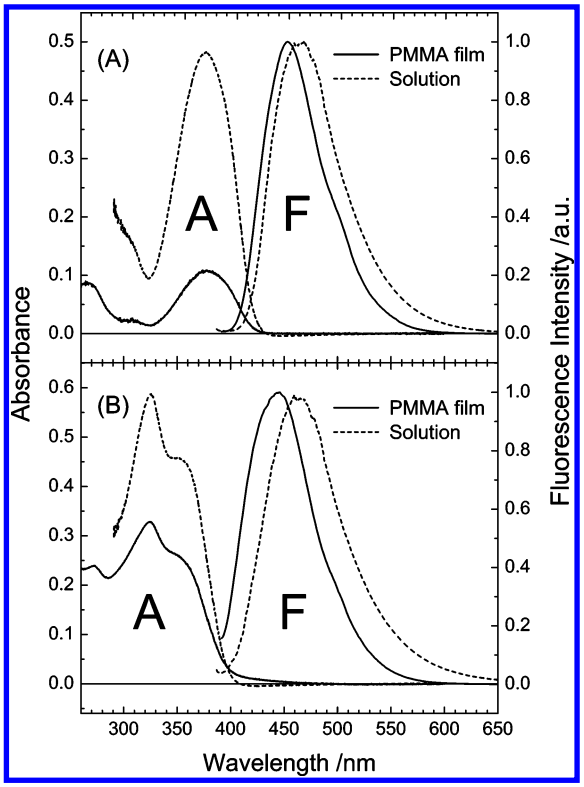

Figure 3. UV/visible absorption and fluorescence spectra of (A) 2,7-DPVTCz and (B) 3,6-DPVTCz in solid films mixed with PMMA (in 1:1000 ratio by mass). The dashed curves are those obtained from solution samples. The maxima of the fluorescence intensities were normalized to 1.0 for comparison.

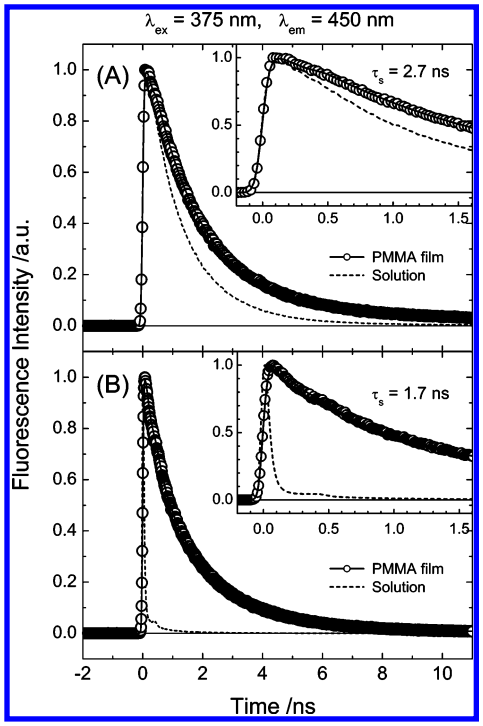

Figure 4. Picosecond fluorescent transients of (A) 2,7-DPVTCz and (B) 3,6-DPVTCz in solid films mixed with PMMA (in 1:1000 ratio by mass) obtained on excitation at $\lambda_{ex} = 375$ nm and probing at $\lambda_{em} = 450$ nm. The dashed curves are those obtained from solution samples for comparison.

spectral feature is different from that of carbazole-based polymers in solid films[20,22] in which red shifts in fluorescence spectra were observed due to interchain interactions between polymer units in the solid state. Therefore, the packing effect due to intermolecular interactions is considered to be insignificant for our carbazole derivatives in the PMMA films.

Because nuclear motion of the molecules is significantly inhibited in a PMMA matrix whereas they are feasible in free solvents, the observed *hypsochromic shift* of the fluorescence spectra in cabazole/PMMA films reflects the influence of molecular motion in a rigid environment that impedes relaxation of the geometry in the excited state. In solution, the excited-state geometries would relax to some extent through certain nuclear coordinates so that the corresponding fluorescence spectra are shifted to the greater wavelength region. The spectral shift for 3,6-linked carbazole is significantly greater than that for 2,7-linked carbazole, implying that the change of the excited-state geometry in solution is greater for the former than that for the latter.

Figures 4A and B display picosecond fluorescence transients of 2,7-DPVTCz and 3,6-DPVTCz in PMMA thin films, respectively, measured with $\lambda_{ex} = 375$ nm and $\lambda_{em} = 450$ nm (Supporting Information, Figures S5−S8, for other transients at $\lambda_{em} = 400-600$ nm); their corresponding transients in solution are shown as dashed curves for comparison. For 2,7-DPVTCz (Figure 4A), we found that the temporal profile in PMMA film shows only slightly slower decay kinetics than that in solution. The transient for the PMMA film is satisfactorily fitted with two exponential decay functions with the small and the large coefficients being 1.8 ns (∼0.9) and 11 ns (∼0.1), respectively; the corresponding relative amplitudes are shown in parentheses. The lifetime of 2,7-DPVTCz in its excited state in a PMMA film is averaged to be 2.7 ns. The transient of 2,7-DPVTCz in solution is dominated by the component for rapid decay, and the change of lifetime of excited states between the two environments is insignificant. In contrast, the temporal profile of 3,6-DPVTCz in PMMA film shows a prominently increased lifetime of its excited state relative to the lifetime in solution (Figure 4B). The transient in PMMA film is fitted with two exponential decay functions with the time coefficients being 0.9 ns (∼0.6) and 3.0 ns (∼0.4) for rapid and slow processes, respectively; the average excited-state lifetime is 1.7 ns. The lifetime of 3,6-DPVTCz in its excited state in solution is less than ca. 30 ps whereas it becomes significantly greater in PMMA film ($\tau_s \approx 2$ ns) when nuclear motion is substantially inhibited in the solid matrix; the discrepancy in τ_s between the two environments is remarkable. This observation is consistent with another 3,6-linked carbazole system (BMVC) in which the intensity of fluorescence was found to increase by 10−100 times when BMVC recognizes DNA in a specific binding site.[11] According to these observations, we conclude that deactivation of a carbazole derivative in its excited state becomes efficient when a key nuclear motion is activated for the system with π-conjugated substituents in the 3,6-position rather than in the 2,7-position.

3.4. Femtosecond Relaxation Dynamics of 3,6-DPVTCz in Solution. Because the decay coefficients of fluorescence transients of 3,6-DPVTCz in solution are too small to be resolved with the TCSPC technique, we performed femtosecond time-resolved experiments for the system using fluorescence up-conversion. The dissolved samples were excited with femtosecond pulses at $\lambda_{ex} = 370$ nm, and the resulting emissions ($\lambda_{em} = 420-560$ nm) were collected through sum-frequency generation (gated pulse at $\lambda = 740$ nm). Figures 5A−D show the femtosecond transients of 3,6-DPVTCz in solution at $\lambda_{em} = 420$, 440, 460, and 480 nm, respectively; the insets show the corresponding transients in a smaller time window (∼5 ps). The transients shown in Figures 5A−C exhibit a double exponential

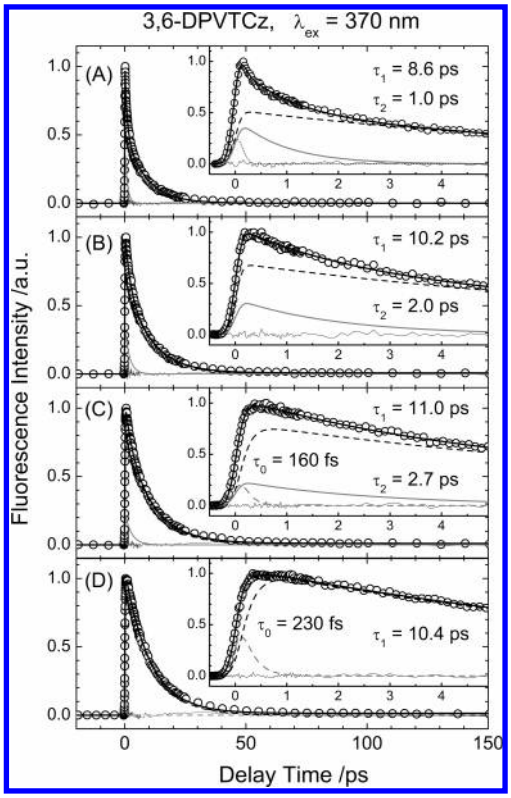

Figure 5. Femtosecond fluorescent transients of 3,6-DPVTCz in dilute toluene solutions ($C = 1.0 \times 10^{-5}$ M) on excitation at $\lambda_{ex} = 370$ nm and probing at λ_{em} (nm) = (A) 420, (B) 440, (C) 460, and (D) 480. The transients were fitted according to an appropriate kinetic model described in the text. The thick solid curves are theoretical fits with residuals shown as thin solid traces; the gray and black dashed curves under each transient are deconvoluted components corresponding to *A* and *B* (in eq 2 or 4), respectively; the gray solid curves shown under the transients represent *B′* (in eq 5). The dotted curve shown in part A results from the interference of the excitation pulse.

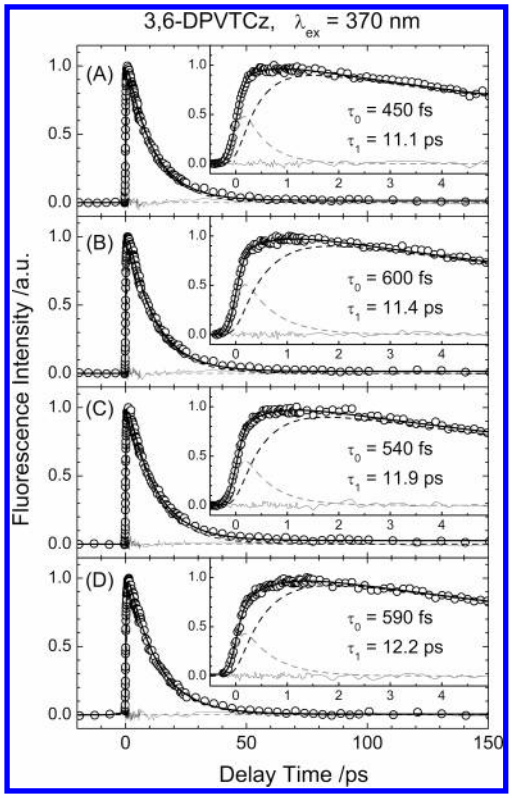

Figure 6. Femtosecond fluorescent transients of 3,6-DPVTCz in dilute toluene solution ($C = 1.0 \times 10^{-5}$ M) on excitation at $\lambda_{ex} = 370$ nm and probing at λ_{em} (nm) = (A) 500, (B) 520, (C) 540, and (D) 560. The transients were fitted according to a consecutive kinetic model as shown in eq 2. The thick solid curves are theoretical fits with residuals shown as thin solid traces; the gray and black dashed curves under each transient are deconvoluted components corresponding to *A* and *B*, respectively.

decay feature: The first decay coefficient τ_1 characterizes the transients at large delays whereas the second coefficient τ_2 characterizes the transients at small delays. For the fit we therefore employed a parallel kinetic model as shown in eqs 4 and 5. The spike signal shown as a dotted curve in Figure 5A ($\lambda_{em} = 420$ nm) results from the interference of the excitation pulse. The values of τ_1 increase slightly from 8.6 ps at $\lambda_{em} =$ 420 nm to 11.0 ps at $\lambda_{em} = 460$ nm, and the corresponding relative amplitudes also increase from 0.54 to 0.77. In contrast, the values of τ_2 increase substantially from 1.0 ps at $\lambda_{em} = 420$ nm to 2.7 ps at $\lambda_{em} = 460$ nm, but the corresponding relative amplitude decreases from 0.46 to 0.23. When the transient is obtained at $\lambda_{em} = 480$ nm (Figure 5D), the second decay component is negligible (the amplitude is too small to yield a meaningful fit), and the first decay component becomes dominant with coefficient τ_1 fitted to be 10.4 ps. Therefore, the second decay component of the transients is observable only in the shorter emission wavelength region, and its amplitude decreases rapidly as the probe window moves to increasing wavelength. The transients obtained at both 460 and 480 nm show slightly a rising feature, indicating that an intermediate species might be involved in these transients; for this reason they were fitted better with two components according to a consecutive kinetic model discussed below.

Figures 6A−D show the femtosecond transients of 3,6-DPVTCz in solution at $\lambda_{em} = 500$, 520, 540, and 560 nm, respectively; the insets show the corresponding transients in a smaller time window (∼5 ps). Because a rising feature is here unambiguously shown at the shorter delays of the transients, a consecutive kinetic model (eq 2) was implemented to fit these transients. As a result, the transients were fitted perfectly with two components: The first component (*A*) decays with a time coefficient τ_0, and the second component (*B*) rises in τ_0 but decays with a time coefficient τ_1. The values of τ_0 were determined to be 160 and 230 fs at $\lambda_{em} = 460$ and 480 nm (Figures 5C and D), respectively, but increased ($\tau_0 = 600$ fs) at $\lambda_{em} = 520$ nm; τ_0 makes no sensible change for λ_{em} greater than 520 nm. The relative amplitudes also alter systematically from 0.44 at $\lambda_{em} = 480$ nm to 0.37 at $\lambda_{em} = 560$ nm, but the value of τ_1 slightly increases from 10 ps at $\lambda_{em} = 480$ nm to 12 ps at $\lambda_{em} = 560$ nm; the corresponding relative amplitude increases from 0.56 to 0.63. *B* is the dominant decay component in the transients shown in Figure 6 with the decay coefficient comparable to that observed in the region of smaller wavelength (Figure 5).

3.5. Theoretical Calculations. We performed quantum-chemical calculations for excited states of model systems to rationalize both the observed large discrepancy in Φ_f and the observed relaxation dynamics between 3,6-DPVTCz and 2,7-DPVTCz. To diminish the computational cost and to make a systematic comparison, we replaced all phenyl groups with saturated hydrocarbons with only one carbon atom to serve as model systems in these calculations. As a result, the model systems contain one ethyl group connected to the central N atom and two dimethylvinyl groups connected to the carbazole core in either the 2,7- or 3,6-position. The optimized geometries of the 2,7- and 3,6-linked species are basically nonplanar with two bridged C−C bonds being twisted substantially: Two bridged

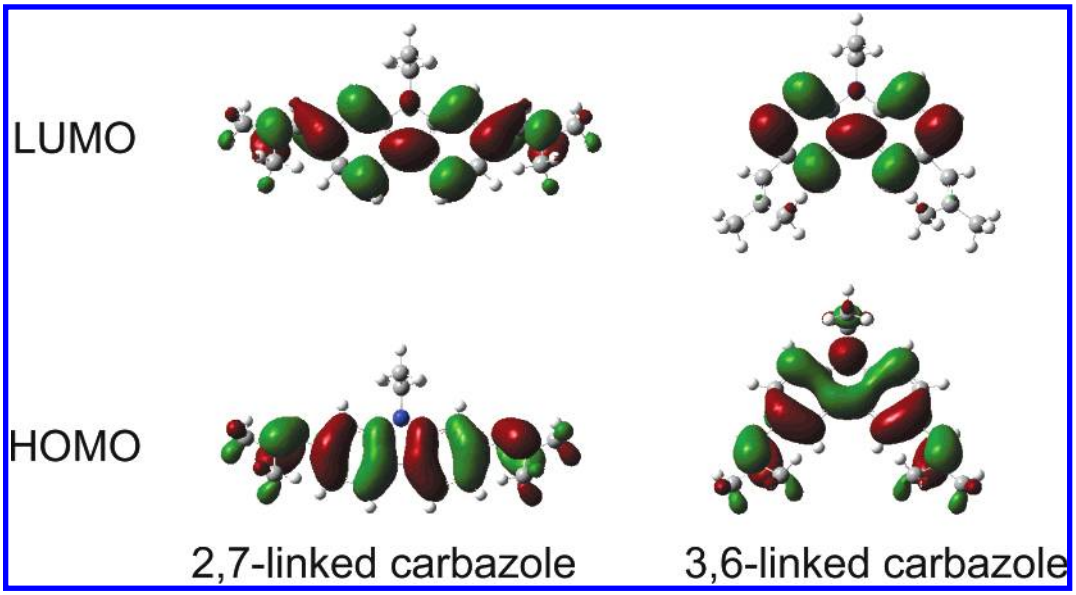

Figure 7. HOMO and LUMO of two dimethylvinylcarbazole derivatives as indicated. The geometries were optimized at the B3LYP/6-31G(d) level of theory.

SCHEME 1: Electronic Resonance Structures of 3,6- and 2,7-Linked Carbazoles in the $^1(\pi,\pi^*)$ State

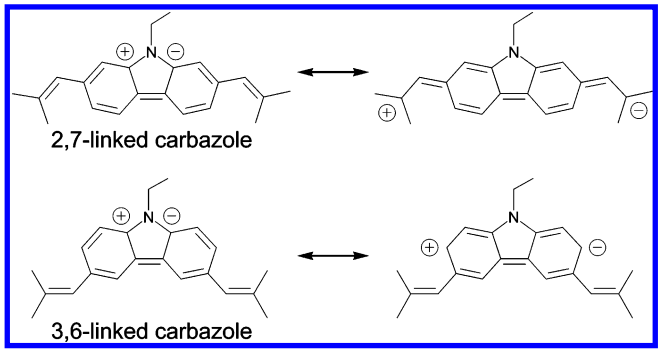

C—C bonds are twisted through a common torsional angle δ = 37−38° for both molecules in the S_0 state. In Figure 7, we show the corresponding HOMO and LUMO of the carbazole derivatives optimized in the S_0 state for comparison. Because electronic excitation from HOMO to LUMO produces the S_1 state, the orbital features shown in Figure 7 might provide important clues to understand the distinct photophysical behavior between the carbazole substituents of the two types. For the HOMO, π-conjugation of the orbitals is effectively extended to the dimethylvinyl groups in both 2,7- and 3,6-linked carbazoles, but the bridged C—C bonds retain a single-bond character in both cases. In contrast, the LUMO shows an extension of π-conjugation over the two dimethylvinyl groups to occur for substituents in only the 2,7- rather than the 3,6-position, which makes the bridged C—C bonds in the 2,7-linked carbazole display a double-bond character. Accordingly, we illustrate the concept of π-conjugation in Scheme 1: The positive and negative charges are completely separable through electronic resonance in the 2,7-linked molecule in the singlet π,π^* excited state,[23] whereas charge separation is localized in only the carbazole core of the 3,6-linked molecule. Hence electron redistribution in the 2,7-linked carbazole causes the original flexible C—C single bond between the dimethyllvinyl moiety and the carbazole core to become a rigid bridge having double-bond character as rotation about the C—C double-bond axis becomes unfavorable in the S_1 state. Localization of the π-conjugation in the carbazole core of the 3,6-linked molecule in the S_1 state does not affect its feasible C—C single-bond twisting motion, thus enabling efficient nonradiative relaxation. We thus expect that rotation about the bridged C—C bonds in the 2,7-linked carbazole is more difficult than in the 3,6-linked carbazole in the S_1 state.

The optimized S_1 minimum (min) structures of 2,7- and 3,6-linked carbazoles are shown in Figures 8A and B, respectively. The two bridged C—C bonds of the former are shorter than those of the latter, which is consistent with the π-conjugation concept shown in Scheme 1. We found that the optimized symmetrical S_1 structure of 2,7-linked carbazole (δ = 27.7°) is a true minimum with all vibrational frequencies being positive numbers (Supporting Information, Documents S1−S2). The optimized symmetrical S_1 structure of 3,6-linked carbazole (δ = 37.5°), however, involves one imaginary frequency (920i cm^{-1}) corresponding to an asymmetrical nuclear motion; further geometry optimization without constraint of molecular symmetry produces an asymmetric structure corresponding to the S_1 (min) of 3,6-linked carbazole with two bridged C—C bonds being twisted by 35.0° and 48.9°, respectively. The symmetrical S_1 structure of 3,6-linked carbazole, S_1 (sym), is therefore considered to act as a transition structure connecting both asymmetric minima on the S_1 PES.

Rotation about the bridged C—C bonds toward a twisted geometry would involve an energy barrier for both model systems because of failure of the extension of π-conjugation in the LUMO for the 2,7-linked carbazole and in the HOMO for both molecules. We classify two reaction pathways through rotation of the bridged C—C bonds: The single C—C twisting reaction path is followed by twisting only one bridged C—C bond and setting the other one free whereas the concerted C—C twisting reaction path is followed by twisting both bridged C—C bonds simultaneously. Because the S_1 PES along either the single C—C twisting reaction coordinate (RC) or the concerted C—C twisting RC is almost flat, a search for the true transition structures on the PES was unsuccessful. Alternatively, we optimized the S_1 structures by constraining the C—C twist angle(s) to 90° and setting the other geometric parameters free. On so doing, the optimized structures of P_1 (only one C—C twisting angle is fixed at 90°) and P_2 (both C—C twisting angles are fixed at 90°) species were obtained. For P_1, the other C—C twisting angles are 22.5° and 35.4° for 2,7- and 3,6-linked carbazoles, respectively. Calculations of vibrational frequencies

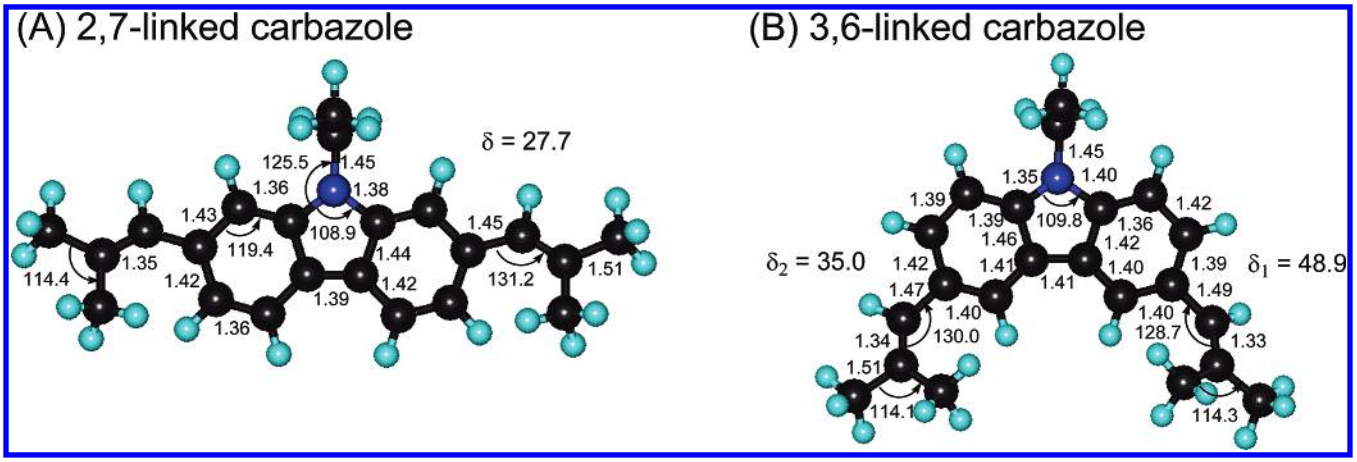

Figure 8. Molecular structures of the S_1 (min) species of (A) 2,7-linked carbazole and (B) 3,6-linked carbazole optimized at the CIS/6-31G(d) level of theory with corresponding bond lengths (Å) and bond angles (deg) as indicated.

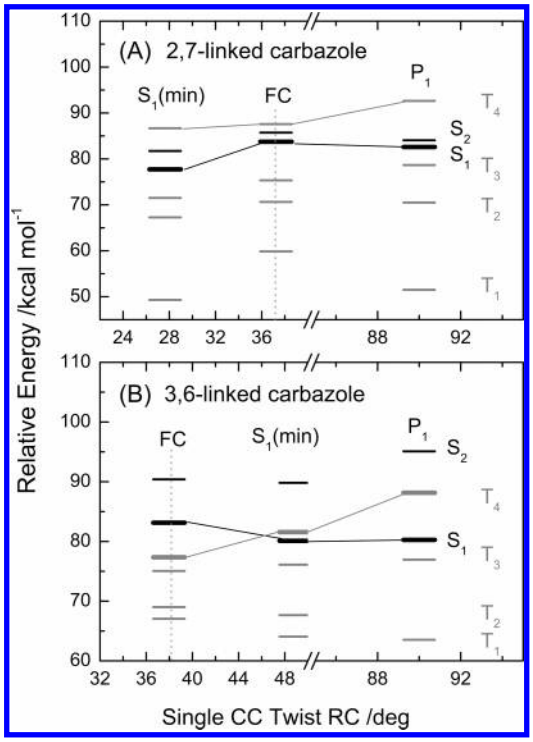

Figure 9. Relative excited-state energies of the FC, S_1 (min), and P_1 species of (A) 2,7-linked carbazole and (B) 3,6-linked carbazole along a single C—C twisting RC calculated at the TDB3LYP/6-31+G(d) level of theory.

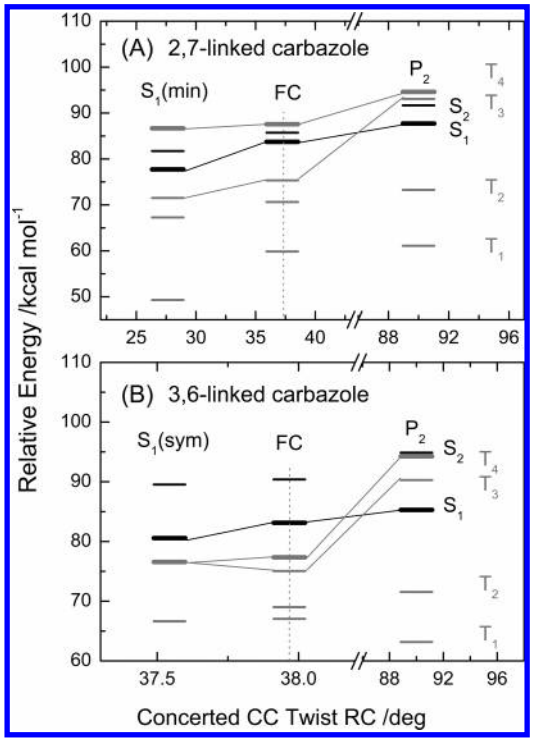

Figure 10. Relative energies of excited states of the FC, S_1 (min) or S_1 (sym), and P_2 species of (A) 2,7-linked carbazole and (B) 3,6-linked carbazole along a concerted C—C twisting RC calculated at the TDB3LYP/6-31+G(d) level of theory.

indicate that there is only one imaginary value corresponding to the twisting motion of the C—C single bond for the P_1 species whereas two imaginary values correspond to one symmetrical C—C twisting motion and the other asymmetric C—C twisting motion for the P_2 species (Supporting Information).

To obtain energetics for an improved understanding of the interaction between surfaces for excited states, we performed single-point energy calculations at the TD B3LYP/6-31+G(d) level of theory, a theoretical model that reproduces the UV spectrum of carbazole molecule,[24] for three key geometries—the FC state, the S_1 (min), and the perpendicular species (P_1 or P_2). Both single C—C twisting (through perpendicular species P_1) and concerted C—C twisting (through perpendicular species P_2) reaction paths are considered; the corresponding calculated results appear in Figures 9 and 10, respectively, in which parts A and B show the results for 2,7- and 3,6-linked carbazoles, respectively. When the single C—C twisting RC is followed from the S_1 (min) to the P_1 region, the energy barrier heights are calculated to be ~5 and ~0.2 kcal mol^{-1} for 2,7- and 3,6-linked carbazoles, respectively. Similarly, the energy barriers along the concerted C—C twist RC are calculated to be ~10 and ~5 kcal mol^{-1} for 2,7- and 3,6-linked carbazoles, respectively. That the calculated energy barrier for twisting the bridged C—C bond(s) is much larger for the 2,7-linked carbazole than that for the 3,6-linked carbazole confirms the π-conjugation concept illustrated in Scheme 1.

3.6. Relaxation Mechanism. On the basis of the results of calculations shown in Figures 9 and 10, we depict the two excited-state RC diagrams (concerted vs single twisting) for 2,7- and 3,6-linked carbazoles in Figures 11A and 11B, respectively. The most prominent discrepancy in the features of the potential-energy curves between 2,7- and 3,6-linked carbazoles is the order of the S_1 and T_4 states: In the FC and the S_1 (min) region T_4 lies above S_1 for 2,7-linked carbazole whereas the order is

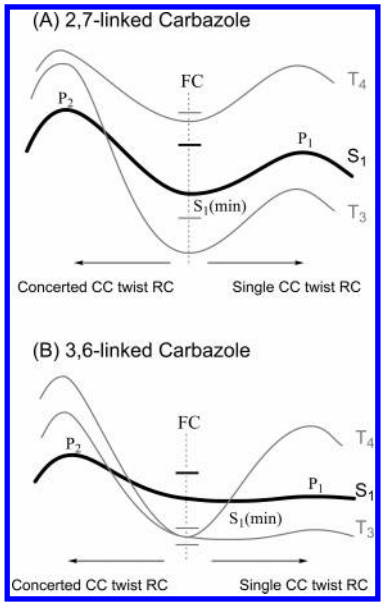

Figure 11. Reaction coordinate diagrams for excited states of (A) 2,7-linked carbazole and (B) 3,6-linked carbazole along the concerted C—C twisting RC (toward the left direction) and the single C—C twisting RC (toward the right direction).

reversed for 3,6-linked carbazole; in the P_1 and P_2 region T_4 is located above S_1 for both molecules. As a result, two notable distinct photochemical features arise. First, moving along the single C—C twisting RC from the FC state toward the S_1 (min) region would cause the potential-energy curves to cross between the S_1 state and the T_4 state in 3,6-linked carbazole, but there would be essentially no curve crossing for the 2,7-linked carbazole. Second, moving along the concerted C—C twisting RC toward the P_2 region would cause the S_1 state to cross both the T_3 and the T_4 states for the 3,6-linked carbazole but to cross the T_3 state only for the 2,7-linked carbazole. Because curve crossing between S_1 and T_4 states is impractical in 2,7-linked carbazole, we expect that the efficient $S_1 \rightarrow T_4$ ISC would be activated only in 3,6-linked carbazole through twisting of the bridged C—C bond(s) in a free environment. The proposed mechanism for efficient ISC deactivation via twisting motions rationalizes that much more rapid dynamics of relaxation (or much smaller fluorescence quantum yield) were observed for the 3,6-linked carbazole than for the 2,7-linked carbazole in solution. When the twisting motions of 3,6-linked carbazole are inhibited in the PMMA film, a greatly decreased rate of relaxation was observed (Figure 4B) because relaxation in the excited state can occur only from the FC state so that efficient ISC via curve crossing would become forbidden in the confined environment.

According to our calculated results, the observed femtosecond relaxation dynamics of 3,6-DPVTCz in toluene solution become rationalized in Scheme 2. The femtosecond pulses at λ_{ex} excite the molecule to its FC state in which geometry relaxation begins on the S_1 PES toward the S_1(min) region. Because FC relaxation produces vibrationally hot S_1 molecules (S_1*) with time coefficient τ_{FC}, the excess vibrational energy would be carried away by solvent molecules with time coefficient τ_{VR}, which eventually makes a cold S_1 species. The emission from both hot and cold S_1 species is observable depending on the probe window (λ_{em}), but it would disappear when efficient electronic relaxation occurs. At greater emission wavelengths (e.g., $\lambda_{em} = 560$ nm) at which a colder S_1 species is probed,[16a] we observed a dominant transient component that rises in τ_0 but decays in τ_1. This observation indicates that the cold S_1 species is produced

SCHEME 2: Relaxation Mechanism of 3,6-DPVTCz in Solution

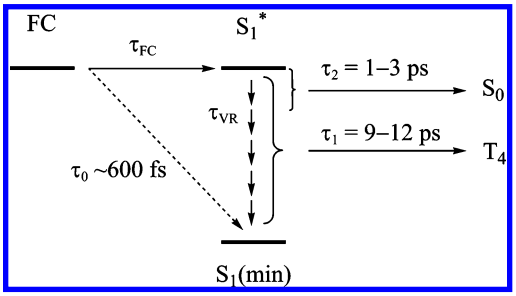

in ~600 fs followed by an efficient ISC deactivation along the single C—C twisting RC in ~12 ps. When the probe window is moved to the smaller emission wavelengths, τ_0 decreases and eventually becomes irresolvable at $\lambda_{em} = 420$ and 440 nm. When the hotter S_1 species were probed at smaller wavelengths (e.g., $\lambda_{em} \leq 460$ nm), we observed an additional transient component that decays in τ_2. Because electronic relaxation becomes more rapid at a smaller λ_{em}, the corresponding deactivation might involve an appreciable energy barrier to be overcome. The observed relaxation period of 1—3 ps is consistent with the duration required for an efficient $S_1 \rightarrow S_0$ internal conversion to occur via twisting the C—C double bond of the vinyl group—an important mechanism for nonradiative deactivation that was observed in stilbene[25] and distyrylbenzene derivatives.[15]

4. Conclusions

Using picosecond time-correlated single-photon-counting and femtosecond up-conversion techniques, we have studied relaxation dynamics of two distyrylcarbazole derivatives, organic compounds for prospective OLED applications, with the 2,2-diphenylvinyl end groups substituted in either the 2,7- or the 3,6- position. We found that 2,7-DPVTCz exhibits intense emission ($\Phi_f \approx 0.6$) with a longer excited-state lifetime ($\tau_s \approx 1.4$ ns) whereas 3,6-DPVTCz shows weak emission ($\Phi_f \approx 0.01$) with a much smaller lifetime ($\tau_s \approx 10$ ps) of its excited state in dilute solutions. Enhanced emission and increased τ_s values were observed for 3,6-DPVTCz encapsulated in a 3,6-DPVTCz/PMMA solid film for which nuclear motions of the molecule are substantially restricted in a PMMA matrix. Calculations on excited states indicate that the $S_1 \rightarrow T_4$ ISC should be considered as an efficient electronic relaxation channel[26] when the twisting motions of the bridged C—C single bond in the 3,6-linked carbazole are feasible. In contrast, this electronic relaxation is inefficient in the 2,7-linked carbazole for the following two reasons: Extensive π-conjugation gives the bridged C—C bond a double-bond character so that a greater rotational barrier is involved in 2,7-linked carbazole than in the 3,6-linked carbazole; curve crossing between the S_1 and the T_4 states would occur along either the single C—C twisting RC or the concerted C—C twisting RC in the 3,6-linked carbazole, but there would be essentially no curve crossing occurring in the 2,7-linked carbazole. Hence we conclude that localization of the π-conjugation and the bridged C—C bond twisting motion on the excited-state surface are responsible for the much smaller values of Φ_f and much more rapid relaxation observed for 3,6-DPVTCz in solution.

Femtosecond relaxation dynamics of 3,6-DPVTCz in solution provide crucial dynamical information to understand the fate of the excited species undergoing FC, vibrational, and electronic relaxations on the S_1 PES. At smaller emission wavelengths, hotter S_1 species were observed, and the corresponding transients

display a biphasic dynamical feature: The rapid component decays in 1−3 ps whereas the slow one decays in ∼10 ps. The rapid component was absent from transients at larger emission wavelengths ($\lambda_{em} \geq 480$ nm) whereas the slow component was retained with an apparent rising feature. The rise-time coefficient was determined to be ∼200 fs at $\lambda_{em} = 480$ nm but increased to a constant value (∼600 fs) at $\lambda_{em} = 520-560$ nm. Therefore, we conclude that after FC and vibrational relaxations the cold S_1 species were observed with the build-up time coefficient ∼600 fs, and then an efficient ISC deactivation, most likely via twisting one of the bridged C−C single bonds, occurs in ∼12 ps. The 1−3-ps relaxation observed only for $\lambda_{em} \leq 460$ nm is assigned to be the $S_1 \rightarrow S_0$ internal conversion occurring via twisting the C═C double bond of the vinyl group.

Acknowledgment. The National Science Council of the Republic of China provided support under Contract No. 94-2113-M-009-016.

Supporting Information Available: Picosecond fluorescence transients of 2,7-DPVTCz and 3,6-DPVTCz in toluene solutions and PMMA films at $\lambda_{em} = 400-600$ nm, a summary of calculated results of 2,7-DPVTCz for FC, S_1 (min), P_1, and P_2 species, and a summary of calculated results of 3,6-DPVTCz for FC, S_1 (sym), S_1 (min), P_1, and P_2 species. This material is available free of charge via the Internet at http://pubs.acs.org.

References and Notes

(1) Kim, D. W.; Moon, H.; Park, S. Y.; Hong, S. I. *React. Funct. Polym.* **1999**, *42*, 73−86.

(2) (a) Morin, J.-F.; Leclerc, M. *Macromalecules* **2001**, *34*, 4680−4682. (b) Morin, J.-F.; Nicolas, D.; Tao, Y.; Leclerc, M. *Chem. Mater.* **2004**, *16*, 4619−4626.

(3) (a) Paliulis, O.; Ostrauskaite, J.; Gaidelis, V.; Jankauskas, V.; Strohriegl, P. *Macromol. Chem. Phys.* **2003**, *204*, 1706−1712. (b) Sonntag, M.; Strohriegl, P. *Chem. Mater.* **2004**, *16*, 4736−4742.

(4) Li, Y.; Ding, J.; Day, M.; Tao, Y.; Lu, J.; D'iorio, M. *Chem. Mater.* **2004**, *16*, 2165−2173.

(5) Zhang, Q.; Chen, J.; Chen, Y.; Wang, L.; Ma, D.; Jing, X.; Wang, F. *J. Mater. Chem.* **2004**, *14*, 895−900.

(6) Thomas, III, S. W.; Swager, T. M. *Macromolecules* **2005**, *38*, 2716−2721.

(7) Wu, F.-I.; Shih, P.-I.; Yuan, M.-C.; Dixit, A. K.; Shu, C.-F.;Chung, Z.-M.; Diau, E. W.-G. *J. Mater. Chem.* **2005**, *15*, 4753−4760.

(8) Chen, C. H.; Shi, J.; Tang, C. W. *Coord. Chem. Rev.* **1998**, *171*, 161−174.

(9) Dias, N.; Jacquemard, U.; Baldeyrou, B.; Tardy, C.; Lansiaux, A.; Colson, P.; Tanious, F.; Wilson, W. D.; Routier, S.; Merour, J.-Y.; Bailly, C. *Biochemistry* **2004**, *43*, 15169−15178.

(10) Silvius, J. R. *Biochemistry* **1992**, *31*, 3398−3408.

(11) (a) Chang, C.-C.; Wu, J.-Y.; Chang, T.-C. *J. Chin. Chem. Soc.* **2003**, *50*, 185−188. (b) Chang, C.-C.; Wu, J.-Y.; Chien, C.-W.; Wu, W.-S.; Liu, H.; Kang, C.-C.; Yu, L.-J.; Chang, T.-C. *Anal. Chem.* **2003**, *75*, 6177−6183. (c) Chang, C.-C.; Kuo, I.-C.; Ling, I.-F.; Chen, C.-T.; Chen, H.-C.; Lou, P.-J.; Lin, J.-J.; Chang, T.-C. *Anal. Chem.* **2004**, *76*, 4490−4494. (d) Chang, C.-C.; Kuo, I.-C.; Lin, J.-J.; Lu, Y.-C.; Chen, C.-T.; Back, H.-T.; Lou, P.-J.; Chang, T.-C. *Chem. Biodiversity* **2004**, *1*, 1377−1383. (e) Chang, T.-C.; Chang, C.-C.; Wu, J.-Y. U. S. Patent 20050090671.

(12) Dierschke, F.; Grimsdale, A. C.; Müllen, K. *Synthesis* **2003**, 2470−2472.

(13) Korneev, S. M.; Kaufmann, D. E. *Synthesis* **2002**, 491−496.

(14) Cha, S. W.; Jin, J.-I. *J. Mater. Chem.* **2003**, *13*, 479−484.

(15) Bhongale, C. J.; Chang, C.-W.; Lee, C.-S.; Diau, E. W.-G.; Hsu, C.-S. *J. Phys. Chem. B* **2005**, *109*, 13472−13478.

(16) (a) Lu, Y.-C.; Chang, C.-W.; Diau, E. W.-G. *J. Chin. Chem. Soc.* **2002**, *49*, 693−701. (b) Lu, Y. C.; Diau, E. W.-G.; Rau, H. *J. Phys. Chem. A* **2005**, *109*, 2090−2099.

(17) Valeur, B. *Molecular Fluorescence*; Wiley-VCH: Weinheim, Germany, 2002; Chapter 6 and other related references therein.

(18) Pedersen, S.; Zewail, A. H. *Mol. Phys.* **1996**, *89*, 1455−1502.

(19) Frisch, M. J.; Trucks, G. W.; Schlegel, H. B.; Scuseria, G. E.; Robb, M. A.; Cheeseman, J. R.; Montgomery, J. A., Jr.; Vreven, T.; Kudin, K. N.; Burant, J. C.; Millam, J. M.; Iyengar, S. S.; Tomasi, J.; Barone, V.; Mennucci, B.; Cossi, M.; Scalmani, G.; Rega, N.; Petersson, G. A.; Nakatsuji, H.; Hada, M.; Ehara, M.; Toyota, K.; Fukuda, R.; Hasegawa, J.; Ishida, M.; Nakajima, T.; Honda, Y.; Kitao, O.; Nakai, H.; Klene, M.; Li, X.; Knox, J. E.; Hratchian, H. P.; Cross, J. B.; Bakken, V.; Adamo, C.; Jaramillo, J.; Gomperts, R.; Stratmann, R. E.; Yazyev, O.; Austin, A. J.; Cammi, R.; Pomelli, C.; Ochterski, J. W.; Ayala, P. Y.; Morokuma, K.; Voth, G. A.; Salvador, P.; Dannenberg, J. J.; Zakrzewski, V. G.; Dapprich, S.; Daniels, A. D.; Strain, M. C.; Farkas, O.; Malick, D. K.; Rabuck, A. D.; Raghavachari, K.; Foresman, J. B.; Ortiz, J. V.; Cui, Q.; Baboul, A. G.; Clifford, S.; Cioslowski, J.; Stefanov, B. B.; Liu, G.; Liashenko, A.; Piskorz, P.; Komaromi, I.; Martin, R. L.; Fox, D. J.; Keith, T.; Al-Laham, M. A.; Peng, C. Y.; Nanayakkara, A.; Challacombe, M.; Gill, P. M. W.; Johnson, B.; Chen, W.; Wong, M. W.; Gonzalez, C.; Pople, J. A. *Gaussian 03*, revision B.5; Gaussian, Inc.: Wallingford, CT, 2004.

(20) Tirapattur, S.; Belletete, M.; Drolet, N.; Leclerc, M. *Chem. Phys. Lett.* **2003**, *370*, 799−804.

(21) Strickler, S. J.; Berg, R. A. *J. Chem. Phys.* **1962**, *37*, 814−822.

(22) Meng, H.; Chen, Z.-K.; Liu, X.-L.; Lai, Y.-H.; Chua, S.-J.; Huang, W. *Phys. Chem. Chem. Phys.* **1999**, *1*, 3123−3127.

(23) Klessinger, M.; Michl, J. *Excited States and Photochemistry of Organic Molecules*; VCH Publishers: New York, 1995.

(24) Tsao, M.-L.; Gritsan, N.; James, T. R.; Platz, M. S.; Hrovat, D. A.; Borden, W. T. *J. Am. Chem. Soc.* **2003**, *125*, 9343−9358.

(25) Baskin, J. S.; Banares, L.; Zewail, A. H. *J. Phys. Chem.* **1996**, *100*, 11920−11933 and references therein.

(26) Another example can be found in the DCM system; refer to C.-W.; Kao, Y.-T.; Diau, E. W.-G. *Chem. Phys. Lett.* **2003**, *374*, 110−118.